Proceedings of ESDA2006
8th Biennial ASME Conference on Engineering Systems Design and Analysis
July 4-7, 2006, Torino, Italy

ESDA2006-95571

NUMERICAL SIMULATION OF WEAR IN RAILWAY WHEEL PROFILES

Abdelrahim S. Abeidi / Politecnico di Torino

Nicola Bosso / Politecnico di Torino

Antonio Gugliotta / Politecnico di Torino

Aurelio Somà / Politecnico di Torino

ABSTRACT

The work describes a method to predict the evolution of the wheel profile of a railway vehicle, depending on the load history acting on the wheelset. The method is based on the determination of the wear on the contact area, which is divided into finite elements according to the strip theory. For each element, in presence of slip, the amount of material loss is evaluated depending on the local value of tangential force and creepage (the meaning of creepage is assumed according to the definition given in [14], [15], [16] as the ratio between the sliding velocity and the tangential rolling velocity). The empirical relation is evaluated according to results of experimental test obtained from literature.

The wear is calculated for the entire contact area superimposing the contribution of each element. The motion of the wheelset in lateral direction causes a motion of the contact patch along the profile. Sequentially, the contact area will acquire a different contact shape and stress distribution. The shape of the worn profile depends on both the load condition and the motion of the wheelset with respect to the track. This profile can be obtained from the new one by subtracting at each time step the material removed from the contact area.

This procedure is simple, but requires variable profiles for each time step, and is not efficient in computational terms.

The strategy proposed here by the authors, is to consider finite periods obtained superimposing several revolution of the wheelset. The worn profile is evaluated in a single step from the cumulative of damage of an entire period. The limitation of this method consists in the different behavior of a wheelset with worn profile respect to a wheelset with new ones, and therefore produces different wear. It is necessary to determine an optimal value for the period to be used to re-evaluate the profile shape, in order to minimize the difference in the predicted shape itself. The method is applied to a suspended wheelset, running on a simulated test track, with S1002/UIC60 profiles. Different periods of re-evaluation of the profiles are considered in order to demonstrate the influence of this parameter.

INTRODUCTION

Wear determines the lifespan of a construction, and in railway applications it affects both rails and wheels, which are the two elements providing guidance and support to the motion of the vehicle. Reduction of wear is therefore one of the important objectives of railway technology; tribology studies are used to develop new design methodologies, in order to reduce wear and increase life of rails and wheels.

Considering the wheel wear, it is important to evaluate not only the total amount of wear, but also the shape variation of the profile. The same amount of wear can cause a higher or lower deterioration of the wheelset performance depending on the new shape of the worn profile. In fact in case of high equivalent conicity, the stability of the vehicle can be heavily reduced.

In general, it is possible to distinguish if the wear is distributed uniformly along the circumferential direction or not. In the last case, unroundness may arise; the wheel is no longer exactly a body of revolution but exhibits waves in the circumferential direction or flatness, this is a problematic type of wear as the rolling stock is severely and dynamically loaded.

This type of wear is usually related to braking operations (wheel flat), or to problems depending on material and loading conditions. Prediction of this type of wear requires a complex numerical investigations involving real time simulations, low time step and precise determination of the loads acting on the wheel. In this work, the study is limited to wear with uniform distribution in the circumferential direction; in this case the wheel remains a body of revolution, but it changes shape in the transversal section.

Wheel-rail wear has been extensively studied over the years. Some of these studies were laboratory tests [1, 2, 3, 4], and some were simulated field experiments [5]. The difficulties and the expenses involved in field experiments force researchers to use, whenever possible, the laboratory tests. However, the major problem was how to transfer these laboratory tests results to the real wheel-rail system.

The problem of wheel-rail profiles design exists for many years and different approaches have been developed to obtain satisfactory wheel-rail profile combination. It is possible to find optimal combination of wheel and rail profile when we deal with closed railway system, i.e. when the same type of rolling stock is running on the same track and no influence of other type railway vehicles presents. Another point is that rail costs much more than a wheel and wheels are quite often re-profiles, so it looks attractive to design a new wheel profile, which matches rail profile. Many researchers have performed wheel-rail wear simulations on the assumption that wear occurs only on the wheel profile, where the rail profile is considered as the steady-state profile. Dynamic forces were calculated using different codes, normal and tangential contact stresses were calculated using Hertzian or non-Hertzian theory and Kalker's codes, and calculations of wear were performed based on the assumption of the linear wear law, i.e. wear rate is proportional to the frictional work "wear index number" [1, 2, 4, 6], and the wear coefficients was generated based on laboratory tests using four roller machine [2], Amsler wear testing machine [1] or twin disc machine [4].

Before describing the main forms of wear, we should point out that the terminology in this field is still not standardized. Although, a glossary edited by DeGee and Rowe (1969) [7], appeared some time ago, it is still not in universal use. However, there are different approaches used for defining the forms of wear as follows:

- Concentrating on the primary cause of each form wear, which has been used in the terminology made by Burwell (1958) [8].
- Examining the surfaces of sliding specimens. This approach may mislead between adhesive and abrasive wear.
- Judging the type of wear by its engineering consequences. Thus, wear may be termed light, medium, severe, galling, etc.

Modern research has established that there are four main forms of wear besides a few marginal processes that are often classified as forms of wear. In the current work, the main forms of wear will be defined according to the concept of the first approach , which differentiates them in adhesive, abrasive, corrosive and surface fatigue wear.

In railways, It is known that wheels undergo wear mostly during traction, climbing a steep track and braking, which in turn increase the interfacial slip. Thus, according to the above mentioned definitions, and supposing that no hard, abrasive matters are present between the sliding surfaces, we can conclude that the most dangerous form of wear on the railway wheels is the adhesive wear. Moreover, the effect of slip will cause the roughen of the surface at the contact area, which will cause the formation of the fragments. This microslip occurs at high local stresses and very small slip velocities and takes place only over a part of the contact zone referred as slip region.

Aim of this work is to develop a method to predict the evolution of the railway wheel profile. Only the adhesive wear process has been considered as illustrated by the experiments of Greenwood and Tabor (1955,1957) [9], [10] who used two-dimensional models of various metals to denote asperities, and then sheared the asperities.

At this time the attention is focused to wear taking place in the tread, during steady state motion of a vehicle.

NOMENCLATURE

A: Contact area, in mm^2.

A_e: Element area, in mm^2.

b: half gauge.

D: Wear depth along lateral direction, in mm.

D_z, D_y: Vertical and lateral components of wear depth, in mm.

K: Wear coefficient.

K_1, K_2: Wear coefficients, 4.8044e-3 & 7.8071e-5, respectively.

N: Vertical Load, in N.

N_{pi}: Number of points considered in the initial profiles.

N_p: Number of points considered in the partial profiles.

pos: Rail inclination angle, 1:20 & 1:40, in radian.

R: Radius of curvature, in m.

r_R, r_L: Wheel rolling radii right and left, in m.

T: Traction force, in N.

y: Lateral coordinate.

Y: Lateral displacement, in m.

U: Total wear rate, in mm/ m rolled.

V: Forward Velocity, in m/s.

W_e: Wear rate per element, in mg/ m rolled.

W_T: Total wear rate, in mg/ m rolled.

z_w, z_r: Vertical coordinate of both Wheel and rail.

α_R, α_L: Contact angles right and left, in radians.

α_0: Average contact angle, in radians.

Δ_{ref}: Reference Penetration = 1.0e-8m

Δt: Time interval, in s.

Δ_z: Perpendicular penetration, m.

Δ_{zw}, Δ_{zr}: Perpendicular penetration of both wheel and rail, respectively, m.

Δ_{zav} : Average Penetration, in m.

ε : Contact angle parameter.

ϕ : Spin creepage, in 1/m.

γ : Creepage on the discrete element [8].

Γ_w , Γ_r : Profiles of Wheel and rail, respectively.

θ : Wheelset rotation around the X (track) axis.

λ : Equivalent Conicity.

η : Lateral creepage.

ρ : Density of wheel material = 7.8 mg /mm3.

ξ : Longitudinal creepage.

1. DESCRIPTION OF THE METHOD

The method developed by the authors is based on the flow chart shown in fig. 1. Vehicle dynamic is evaluated using an MBS code (Simpack) in order to obtain the wheelset displacement, the creepage values, the normal load at each time step. Those data are used by the Contact Module in order to calculate the Friction forces (Required to close the "dynamic loop" within the MBS code) and to evaluate the stress distribution in the contact patch, which is discretized according the FASTSIM [8] algorithm.

Stress and creepage distribution is used by the wear module in order to evaluate the worn profile which is updated at each time step.

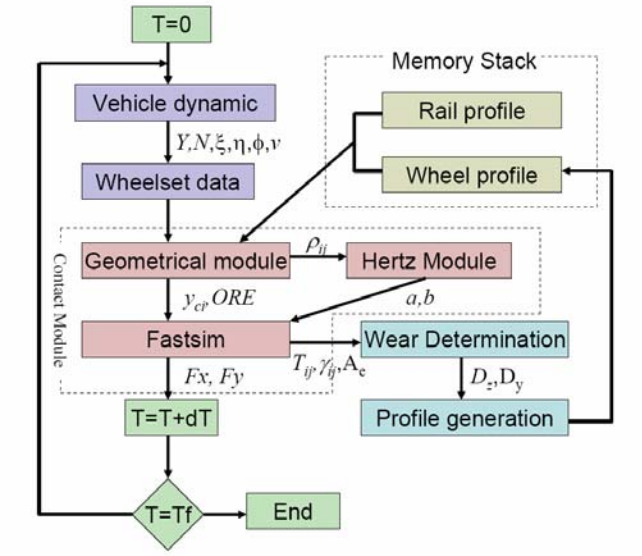

Figure 1: Flow chart of the method: real time process.

This process configure a real time algorithm and require a lot of computational time and the description of the entire track to determine the worn profile of the wheelset. Therefore a more efficient process has been defined (figure 2).

In this case the dynamic analysis is performed off-line on a "reference track" in order to obtain a time history for all the parameters of interest. Those data are then statistical analyzed and average parameters are obtained in order to describe the track with a small number of data.

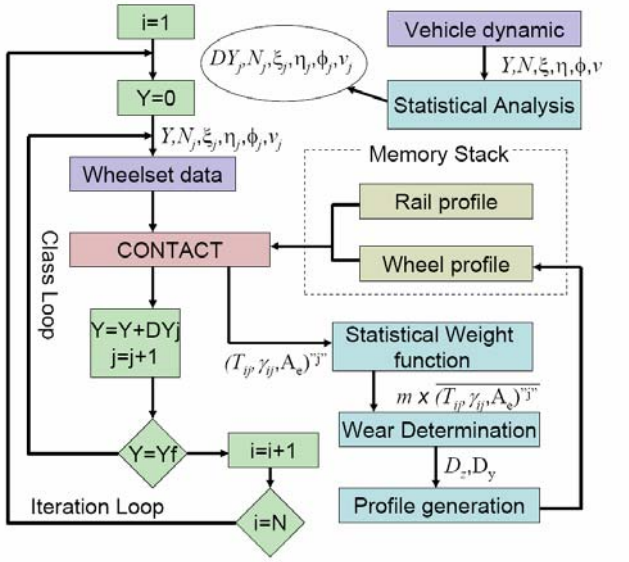

Figure 2: Flow chart of the method: statistical approach. time process.

The principle here used is to divide the points of the time history in a small number of class, each one containing numerical points having similar effect on the profile wear. Therefore the class are formed dividing the lateral displacement of the wheelset in fixed interval DY_j. All point belonging to the same class are supposed to be represented by the average value of creepages and normal load calculated on the entire interval.

The division in class has been performed using different approaches that will be described in detail later on.

The worn profile is generated with a "class loop" applying subsequently the contribution of each class which must be weighted by the class numerosity.

This method allows to simulate track longer than the one analyzed using the Multibody code, simply multiplying the worn depth Dz and Dy by a multiplier *m*.

In this way the profile is worn in a single step and the result may be non realistic, since the worn profile has a different behavior than the newer.

To solve this problem the cycle (describing the same track) can be repeated *N* times changing the profile (Iteration Loop) at each iteration. A good compromise can be achieved comparing different combination N x m to obtain the same track length (of course with m=1 the simulation is a real-time simulation).

1.1 Geometrical Problem

The most critical part of the code is related to the contact point determination, which has been improved respect the one developed by the Authors in [12]. In fact it is mandatory to improve the numerical efficiency of the method a to be able to

manage real profile. The algorithm code here described, developed within the MATLAB code, was intended to locate the contact points on both wheels simultaneously, and to calculate all the required geometrical parameters (curvatures, ORE parameters [17] …).

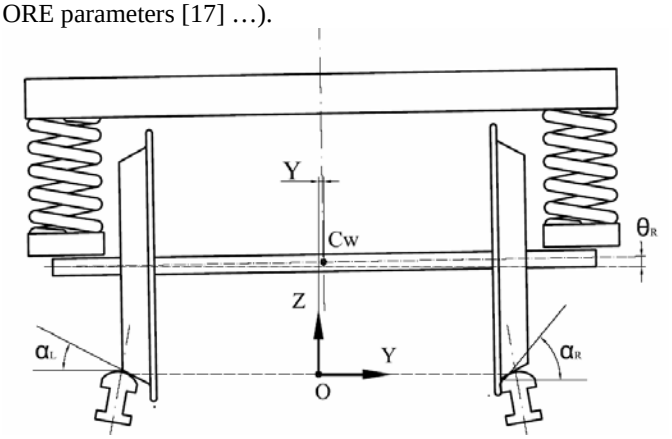

Figure 3: Reference system.

The problem has been investigated as two-dimensional, therefore is known that result may be inaccurate on narrow curve or for large angle of attack in particular on the flange, due to the contact point shift here not represented [13]. Cartesian coordinate system y , z with its origin at the track center line is used, as shown in Fig 3.

The original wheel and rail profiles, which are S1002 and UIC60 respectively, are represented in the zy plane with origin in the center of the track O and equally divided into N_{pi} points in the y (lateral) direction.

Hence, to reduce the calculating time, only the interested parts of the wheel and rail profiles are considered and, divided again into less number of n-points, N_p. The profiles are then approximated using a left-side parabolic interpolation; it is based on the idea of interpolating the profile between two consecutive discrete points of the profile, using a parabola defined on three consecutive points starting from the left side.

The entire profile of wheel (w) and rail (r) can be easily defined using the equations:

$$z_{w,i} = a_{w,i} y^2 + b_{w,i} y + c_{w,i} \quad (1).$$

$$z_{r,i} = a_{r,i} y^2 + b_{r,i} y + c_{r,i} \quad (2).$$

Where the a, b ,c coefficients define a "shape" matrix for each profile. This approach allow an easy analytical calculation of the contact points and curvatures.

To evaluate the contact points the equations (1) and (2) can be simply subtracted on the entire profiles in order to find the penetration Δ_z:

$$\Delta_z = z_w - z_r \quad (3).$$

This value has to be corrected considering only the penetration component along the perpendicular direction to the profiles. Since the profiles are not tangent in general, except in the contact point which is not yet located, we have defined the average penetration, Δ_{zav}, is determined, as follows:

$$\frac{dz}{dy} = \tan\alpha \quad (4).$$

$$\Delta_{zw} = \Delta_z \cdot \cos(\alpha_w) \quad (5).$$

$$\Delta_{zr} = \Delta_z \cdot \cos(\alpha_r) \quad (6).$$

$$\Delta_{zav} = (\Delta_{zw} + \Delta_{zr})/2 \quad (7).$$

The contact point is then found by a discrete minimization of the penetration between theses points. This minimization is based on rotating and translating the wheel profiles and, the condition that controls it, is:

$$\Delta_z \geq \Delta_{ref} \quad (8).$$

To find the contact point an iterative procedure is used. At first the actual maximum penetration is calculated both on the left and right side. Then a roto-translation is applied on the wheelset in order to obtain DZ=0 in both side. Since the roto-translation is defined according to simple triangulations and the profile are non linear, the result require several iterations.

The process has been optimized in case of the statistical approach where the wheelset, due to the class loop of figure 2, is moved monotonically in the lateral direction. In this case, the starting condition for each iteration is calculate as follow:

$$z_t = 2 \cdot z_{t-1} - z_{t-2} \quad (9).$$

$$\theta_t = 2 \cdot \theta_{t-1} - \theta_{t-2} \quad (10).$$

After the first iteration of the external loop (iteration loop in fig. 2), the starting condition is considered equal as the previous value obtained in the same position.

With this approach is possible to achieve convergence (error lower then 1E-6 m) after 12 iteration on the flange in the worst case and 2-3 iteration in the tread.

The, the radius of curvature and the contact angle at each contact point can be calculated by the following relations, respectively:

$$\rho = \left(1 + \left(\frac{\partial z}{\partial y}\right)^2\right)^{3/2} \Bigg/ \frac{\partial^2 z}{\partial y^2} \quad (11).$$

$$\alpha = \tan^{-1}\left(\frac{dz}{dy}\right) \quad (12).$$

The contact angle for each side is found by taking the average value of α_L, α_R.

In order to predict the dynamic behavior of the wheelset, in case of real profiles, it is possible to use a set of equivalent geometrical parameters. In this work, according to [12], the ORE parameters (defined by [16]) have been used:

$$\lambda = (r_L - r_R)/Y \quad (13).$$

$$\alpha_0 = (\alpha_L + \alpha_R)/2 \quad (14).$$

$$\varepsilon = (\alpha_L - \alpha_R) \cdot b/Y \qquad (15).$$

Those parameters must be evaluated for each lateral position of the wheelset.

Considering a rail inclination (pos) equal to 1:20 a comparison has been made of some parameters with results obtained from [11] and, reasonable concordance achieved. The next graphs show some of these results:

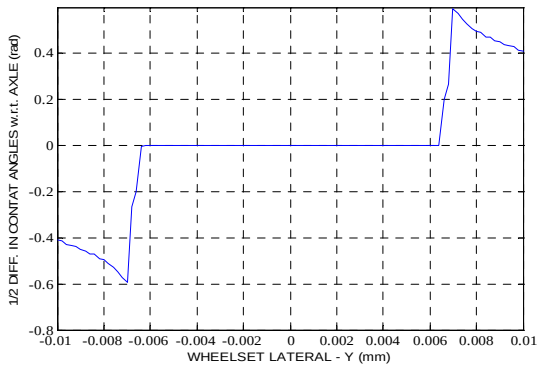

Figure 4: Half-contact angle difference

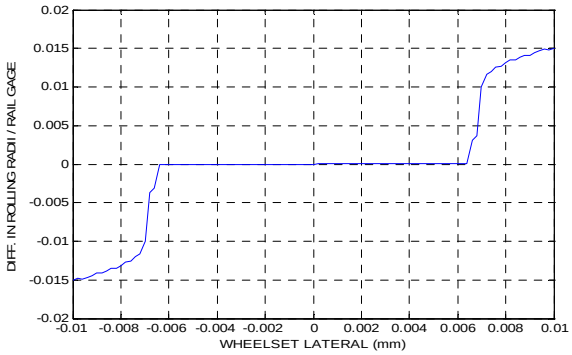

Fig.5: Normalized rolling radii difference

The following graphs show the variation of α_0 with Y, and a comparison between different rail inclination angle is illustrated.

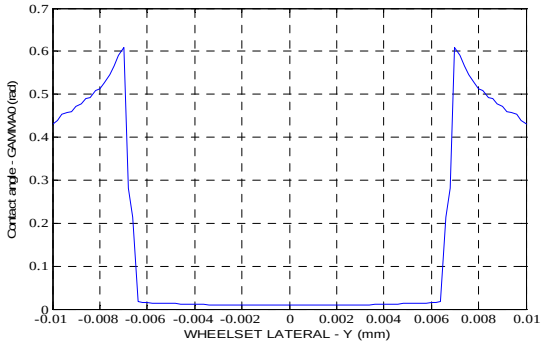

Fig.6: Equivalent contact angle variation at $pos = 1:20$

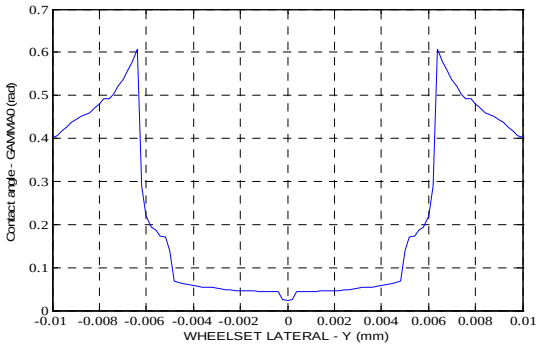

Fig.7: Equivalent contact angle variation at $pos = 1:40$

1.2 Contact Area / stress determinations

The contact problem has been approached according to the method developed by the authors as described in [12.]. The geometrical solution as been improved as shown in §1.1. This has been necessary in order to allow a faster determination of the contact points and to be able to change the profiles during the simulation.

The Contact area has been calculated according the Hertz theory using an elliptic contact patch. Tangential stresses are evaluated using the Simplified Theory developed by Kalker (Fastsim algorithm) [8], but the method can be applied to any contact formulation using a finite discretization of the contact area.

The following Figures (8, 9) show the variation of the tangential stress and the pressure distribution at an arbitrary chosen contact point on the flange border of the right wheel in presence of lateral and longitudinal creepage.

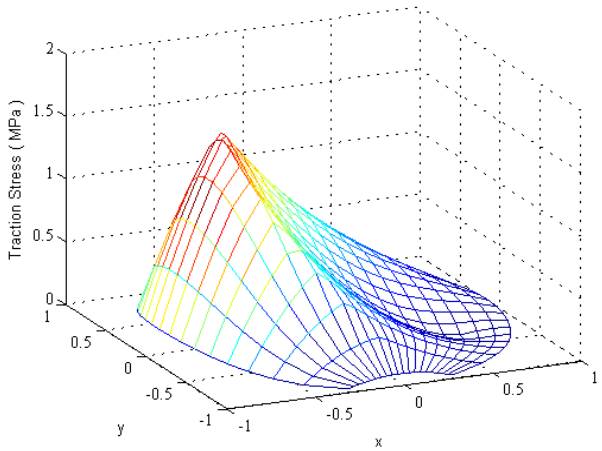

Fig. 8: Tangential stress in the contact area.

The tangential stresses are obtained using the strip theory (Fastsim [8]) with a constant friction coefficient equal to 0.36. Due to the presence of the kinematical creepage, the contact area is divided in a portion, close to the leading edge, where sliding occurs (local tangential stress = Normal stress x friction

coeff.) and a portion characterized by adhesion (local tangential stress < Normal stress x friction coeff.).

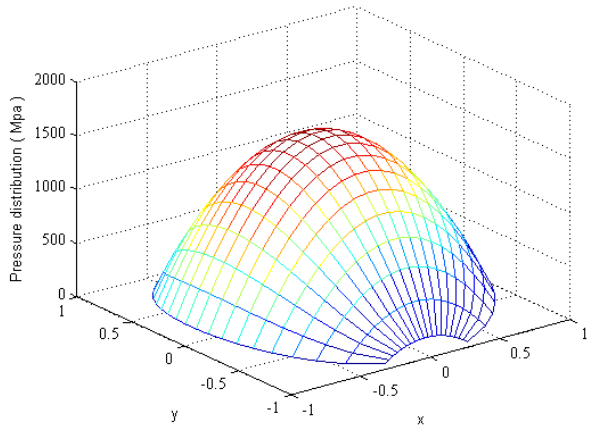

Fig. 9: Pressure distribution over the contact area.

Only the sliding portion of the contact area will be considered to predict the profiles wear.

1.3 Wear determination

Based on the mentioned definitions of wear, we have considered the presence of only the adhesive wear form in the slip region of the contact area. But according to [1], the wear forms were classified as type I, II and III, which could be summarized as follows:

- Type I wear: it was found that the wear rates were independent of the material composition and, of the creepage provided that the limiting coefficient of friction had been achieved. The wear modes operated in this regime are oxidative and deformed manganese sulphide inclusions-associated flake formation.
- Type II wear: it was found that the wear rate was dependent on the material properties and varied with both the applied contact pressure and creepage. Therefore, the wear rate could be calculated by means of the proportionality law of wear and friction work done, which can be described as follows:

$$Wear\ rate = K \cdot {}^{T \cdot \gamma}\!/_{A} \qquad (15).$$

This wear mode was described as a plastic deformation over a number of contact cycles followed by a shear fracture which generates a completely metallic flake-like particle. Therefore, it is sometimes described as adhesive wear.

- Type III wear: Beyond a creepage of 10% a dramatic changes occurred in the wear rates. These were caused by the transition from type II to type III wear , which causes a breakdown in the relation between wear rates and $T\gamma/A$ encountered in type II.

However, we consider in the determination of the wear rate the results obtained for type II wear, which will not be accurate when the creepage exceeds 10%. Based on these results, we derived a relation for the determination of the wear rate in $\left(mg \cdot mm^{-2} \cdot m^{-1} rolled\right)$, as follows:

$$wear\ rate = K_1 \cdot (T\gamma/A) + K_2 \cdot (T\gamma/A)^2 \qquad (16).$$

Then, wear constants K_1 and K_2 was determined and the relation is plotted as shown in Fig. 10, according to the experimental data given by [1]. Using the strip theory and FASTSIM algorithm, the contact area was divided into $m \times n$, (20x20 is used for all calculations in this work), elements and the creepage γ, the traction force T and the area A was calculated for each element. The wear rate W_e, as shown in Fig. 11 and 12, for each element in the slip region was calculated.

$$W_e\left(\frac{mg}{m\,rolled}\right) = \left(K_1 \cdot (T\gamma/A)_e + K_2 \cdot (T\gamma/A)_e^{\,2}\right) \cdot A_e \qquad (17).$$

The sum of the wear rates for all the elements in the rolling direction, gives the wear rate W_T for a lateral portion of the wheel profile (dy) and must be evaluated for each section in the lateral direction:

$$W_{T,i} = \sum_x W_e \qquad (18).$$

To calculate the worn depth D along the normal direction (U_i), we have divided $W_{T,i}$ by the density and wear has been distributed along the entire circumferential length of the wheel as follows:

$$U_i\left(\frac{mm}{m\,rolled}\right) = \frac{W_{T,i}}{\rho \cdot 2 \cdot \pi \cdot r \cdot dy} \qquad (19).$$

Then the component in lateral and vertical direction can be calculated from the normal depth considering the contact angle.

$$D_{z,i}(mm) = U_i \cdot V \cdot \Delta t \cdot \cos\alpha \qquad (20).$$

$$D_{y,i}(mm) = U_i \cdot V \cdot \Delta t \cdot \sin\alpha \qquad (21).$$

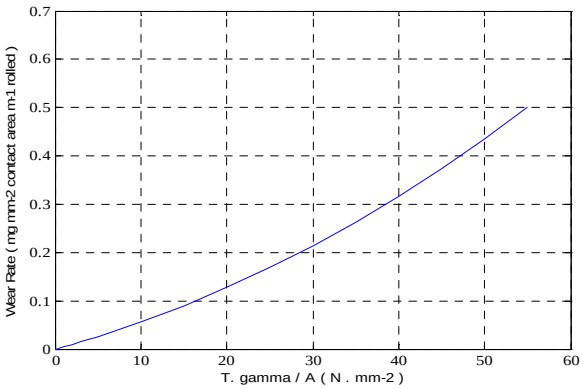

Figure 10: Type II wear rate plotted against $T\gamma/A$ for type D steel wheel.

Examples of the wear rate and the corresponding wear depth are plotted, see fig. 13, at lateral wheelset displacement of 4.7 mm, for a rail inclination angle of 1:40 and, at the first cycle. It is obvious that the wear rate is calculated along the normal to the contact point.

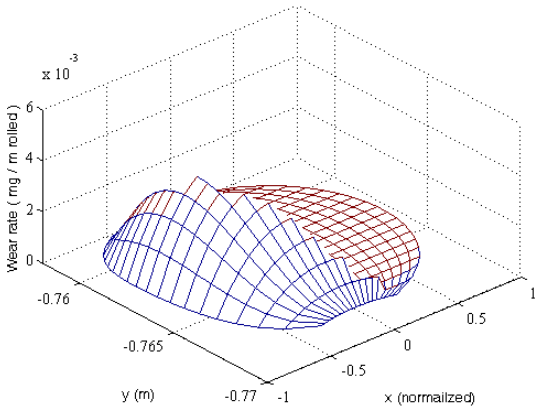

Figure 11: Mass worn away of L-wheel at lateral displacement of 4.7 mm.

Therefore, there will be two components of the wear depth along the y and z directions. But, due to the fact that our procedure is based on equally dividing wheel profiles in the y-direction, the y-component of wear depth cannot be considered easily. Neglecting the lateral depth of wear, in the considered example, there is an error in calculating the wear depth of around 0.87% at the L-wheel contact, since the contact occurred on the tread. While at the R-wheel contact, the error has a significant value of around 12.4% and this is due to the fact the contact occurred near the border of the flange.

But, in case of using rail inclination angle of 1:20, we found that the error for the same case is around 1.26% for both wheels, because the contact occurred on the tread at both sides.

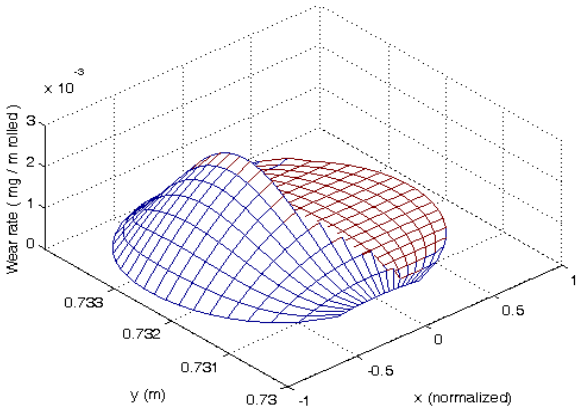

Figure 12: Mass worn away of R-wheel at lateral displacement of 4.7 mm.

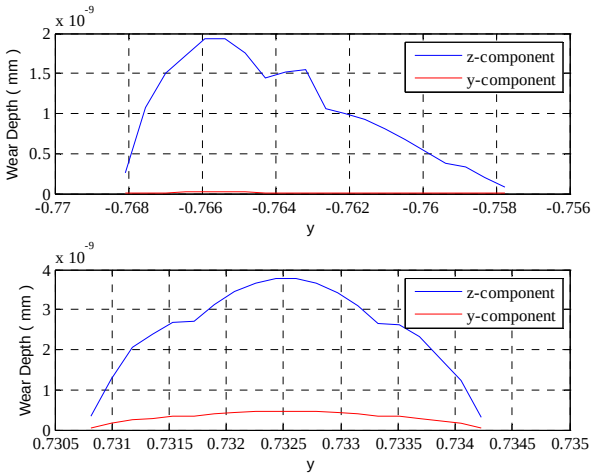

Figure 13: Wear depth of L-wheel (up) and R-wheel (down) at lateral displacement of 4.7 mm.

1.4 Generation of the new profile

Thus, the worn depth at the contact area can be obtained for each wheel profile. By using the spline interpolation, the worn depths at the specified contact areas will be subtracted from original profiles in the z-direction.

The amount of wear can be magnified by using a multiplier m, equal to 1 (real-time), 10,100,1000, ….

These newly generated wheel profiles will be stored and used to continue the simulation.

This procedure will be repeated for the whole time history of the distance rolled according with the flow chat of fig.1 and fig. 2. Of course to use an high multiplier reduce the computational time, but also reduce the accuracy of the simulation. Therefore it is important to calculate an optimal value of the multiplier to achieve a compromise between accuracy and computational time.

1.5 Long term damage simulations

Since the calculation time will be very long if the real time iteration is applied. Five different methods have been used to determine the long term damage in order to reduce the time and, to preserve accuracy, as follows:

Constant Parameters - Method I:

This method is very simple. All the parameters; ξ, η, ϕ, Y, V and N are considered constants by taking the average value of each one along the time history.

Statistical Fixed Interval Lateral Class - Method II:

The lateral displacement of the wheelset is divided in interval (“class”) with fixed width. The points on the time history fall arbitrarily on the various classes that have different numerosity. The interval used is 0. 2 mm, and all the other parameters are

calculated for each interval by taking the average value. The wear calculated on each class must be weighted depending on the numerosity. The number of classes resulting from this method are 56, as shown in Fig. 14. Considering the track data, we found that some parameters have two peaks at the same class, and this of course causes an error in taking the average value. An example is illustrated in Fig. 15, which shows the distribution of two parameters at the class 56 for the left wheel, with a lateral displacement of 5.45 mm.

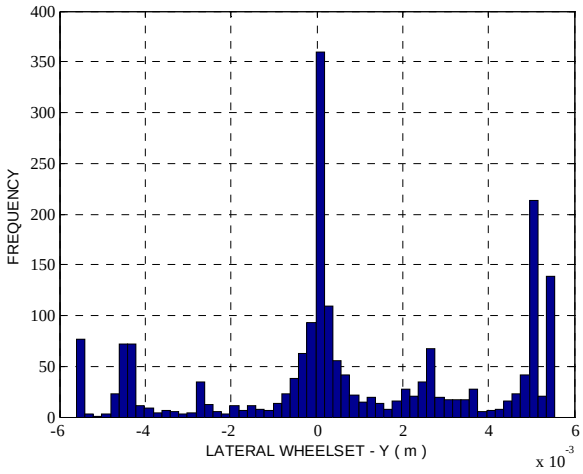

Figure 14 Fixed interval lateral class

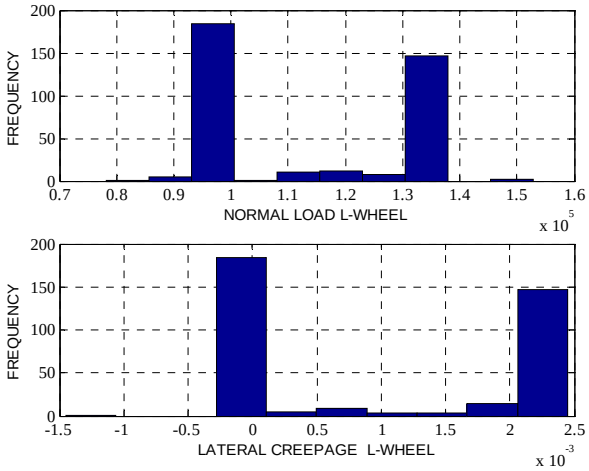

Fig. 15 Distribution of η and N at the class 56 for the L-wheel

Statistical fixed number of points class (over time) – Method III:

The time history in this method was divided into equal 50 periods of 0.65s, which is 40 points class, but the displacement Y was not ordered. The average value of all the parameters was calculated statistically including Y.

This method can be accurate if the evolution of the parameters (including Y) evolves slowly, but in case of wide dispersion of the data on the same class (for example in presence of track irregularities) the results can be inaccurate..

Statistical Fixed Number of Points Class (Over Lateral Displacement) – Method IV:

In this method the lateral displacement was divided in class with fixed numerosity. In this way the informations regarding the position along the profile are used at best, but the historic order of application is completely lost.

The method can be inaccurate if stresses are concentrated in defined period of time (braking) and are accurate for random dispersion.

Thus, this method should be more accurate than the others. Firstly, the data was arranged in ascending order of the lateral wheelset Y. Then 40 points per class were considered in order to have Fifty classes, as shown in Fig. 16, which of course reduces the computational time. The data was recalculated by taking the median value at each class.

By examining the distribution of the parameters, we found that almost no double peak occurs. Therefore, our assumption of taking the median value can lead to a more precise results.

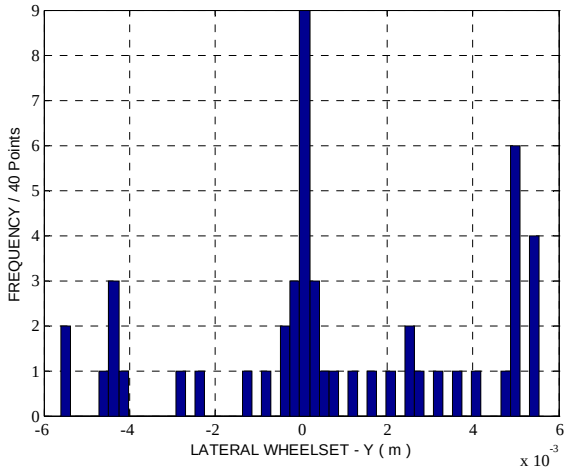

Figure 16: Fixed number of points class

2. SIMULATIONS

The method has been applied to calculate the worn profiles of a wheelset running on a reference track. The dynamic behavior of the wheelset has been obtained by numerical simulations performed with the Simpack MBS code.

Simulations are not used to predict the real development of the worn profiles, but in order to compare different approach as described in the previous chapter.

At first, the evolution of the profiles is compared while using constant parameters, different statistical approaches or real time simulation.

Later, the effect of track irregularities and vehicle velocity is investigated.

2.1 Track data

The track used in the simulation is a portion (1.33 Km) of a real Italian secondary line composed by:

Segment 1: Straight track, length = 200 m
Segment 2: Clothoid, length 90 m.
Segment 3: Curve, Radius = -1040 m, length 200 m, superelevation -90 mm.
Segment 4: Clothoid, length 90 m.
Segment 5: Straight track, length = 175 m
Segment 6: Clothoid, length 75 m.
Segment 7: Curve, Radius = -500 m, length 29 m, superelevation= -150 mm.
Segment 8: Clothoid, length 75 m.
Segment 9: Straight track, length = 49 m
Segment 10: Clothoid, length 65 m.
Segment 10: Curve, Radius = 588 m, length 124 m, superelevation= 130 mm.
Segment 11: Clothoid, length 65 m.
Segment 12: Straight, length 117 m.

The first simulations are performed considering the theoretical track. In §2.10 the simulations are performed in the same track with superimposed the track irregularities in the vertical lateral and roll direction measured on the real track every 600 mm.

2.2 Vehicle data

The method is applied to the first wheelset of a Y25 bogie with an axle load of 20 tons. The bogie belong to a freight vehicle disposed as first trailed vehicle of a short convoy (6 vehicles and a Bo-Bo-Bo locomotive). The vehicle moves along the track at a constant speed of 40 m/s (the maximal velocity of this vehicle).

2.3 Profiles data

The new wheel profile used for the simulation is the S1002 applied on a 0.46 m radius wheel.
The profile is paired with a UIC60 rail profile seated with an inclination angle of 1:20 and 1:40. The wheel profile change during the simulations due to the wear process, while the rail profile remains new.

2.4 Simulation plan

The simulations performed in this work can be summarized on table 1. In addition, using the statistical method with fixed number of points per class (over lateral displacement) and multiplier 100, the simulation is repeated considering measured track irregularities. Finally, the same simulation (with no irregularities) is performed at different speed (10 and 20 m/s).

Method	Rail incl.	Wear Multiplier	Distance [km]
Constant parameters - I	1:40	1000	130000
		100	13000
		10	13000
	1:20	1000	130000
		100	13000
		10	13000
Statistical fixed interval class - II	1:40	1000	260000
		100	130000
		10	13000
Statistical fixed number of points class (over time) - III	1:40	1000	13000
		100	13000
Statistical fixed number of points class (over lateral displacement) - IV	1:40 & 1:20	1000	13000
		500	13000
		400	13000
		200	13000
		100	13000
		10	13000
	1:40	100	350000
		10	13
	1:20	400	130000
Real time	1:40	1	13
		1000	13000
	1:20	1	10

Table 1: Simulation plan

2.5 Wear prediction using constant parameters simulations – Method I:

An example will be illustrated, see figure 17, to show the evolution of wear, the effect of the rail inclination angle and the wear rate.

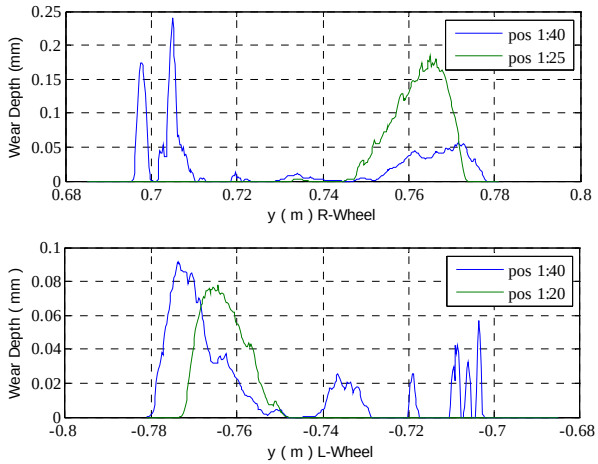

Figure 17. Wear depth evolution after 130000 km on the right (up) and left (down) wheel profile with different rail inclinations.

A 130000 km simulation has been considered. Studying the results, it is clear that the wear with the angle 1:20 progresses on the face only, while with the angle of 1: 40 the wear occurs also at the flange. Obviously, the wear rate on the face with 1:40 is lower than that with 1:20 for the R-wheel, and almost the same on the L-wheel.

2.6 Wear prediction using statistical approach with fixed interval (lateral) class – Method II:

In this method, the illustrative example selected shown in Fig.18 is with a rail inclination angle of 1:40, 150000 km, 100 multiplier and for both wheels.

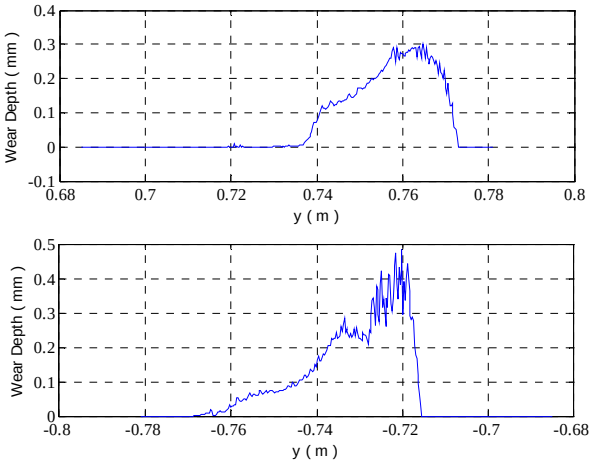

Figure 18. Wear depth for both wheels after 150000 km with 1:20 rail inclination angle.

We can notice that at the R- wheel the maximum amount of wear occurs at the face and no wear appears at the flange border, while on the L-Wheel the wear is more at the flange border. Moreover, the maximum wear depth is almost the same neglecting the error caused by the multiplier.

2.7 Wear prediction using statistical approach with fixed number of points (over time) class – Method III:

A 13000 km, multiplier 10, R-wheel and with an inclination angle of 1:40 is considered to show the wear evolution using this method. The results here shows a completely different behavior as compared with method II, but although it shows a coincidence with method I in the way of progression of wear, the wear rate is higher because of using constant parameters in method I, see Figure 19.

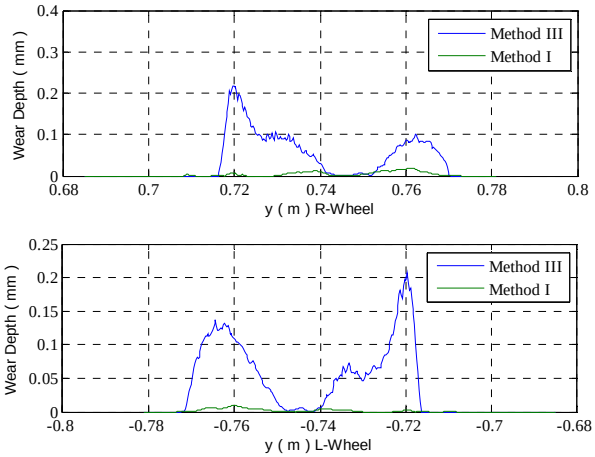

Figure 19: Comparison between Method I & III of wear depth evolution after 13000 km on both wheel profiles.

2.8 Wear prediction using statistical approach with fixed number of points (lateral) class – Method IV:

This method will be deeply studied as it gives more accurate results from the statistical point of view, as explained before.

First, we will consider the general case of 13000 km with Both 1:20 and 1:40 rail inclination angles to study the wear evolution and the wear rate, see fig. 20.

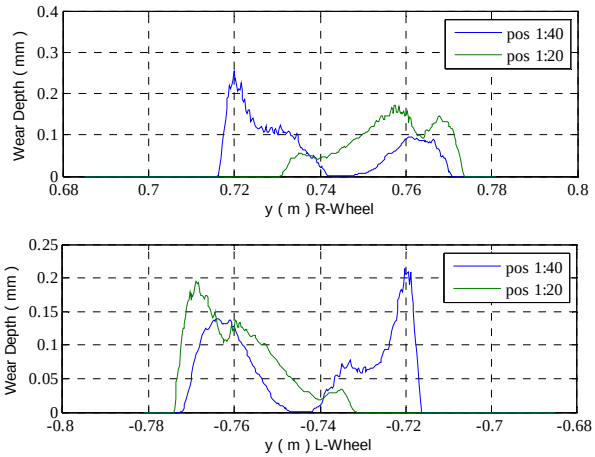

Figure 20: Wear depth evolution after 13000 km on the both wheel profiles.

In fact, It shows that the evolution of wear is symmetrical on both wheels though the wear rate is different, which of course is due to the variation of the creep and the traction forces. A simulation of long distance (130000 km), and with

100 multiplier has been performed to show the shape of the worn profiles with both 1:20 rail inclination angle as in fig. 21.

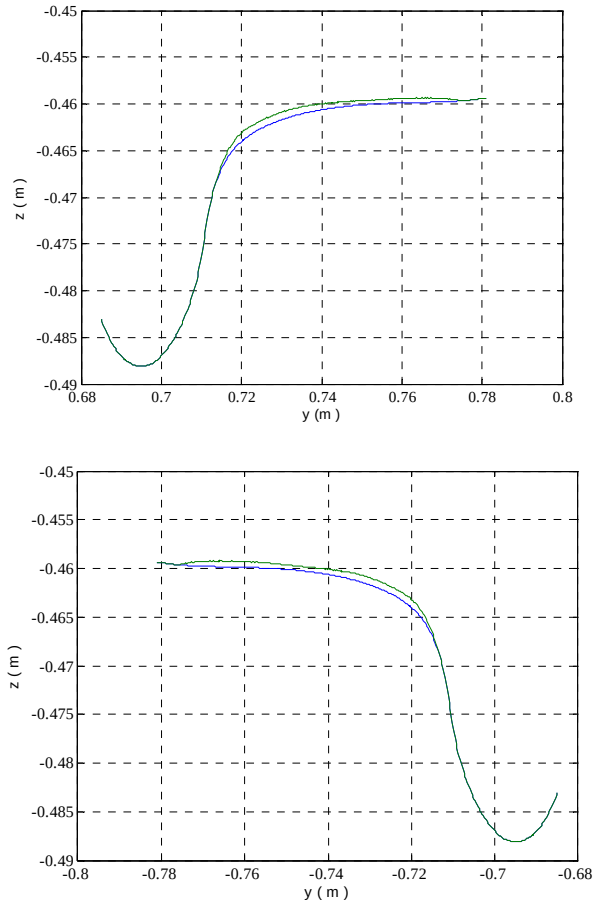

Figure 21: Comparison between new and worn profiles of both wheels with 1:20 rail inclination angle.

2.9 Wear prediction using real time simulation:

In this simulation, we have considered only 13 km, because it is time consuming method. But it is evident that the wear evolution is the same as the one obtained from Method III and IV. Moreover, a 13 km simulation was done with IV method with 1:40 rail inclination angle and 10 multiplier. Actually the results are almost identical and were plotted in Fig.22, which confirms that method IV gives the accurate progress of wear.

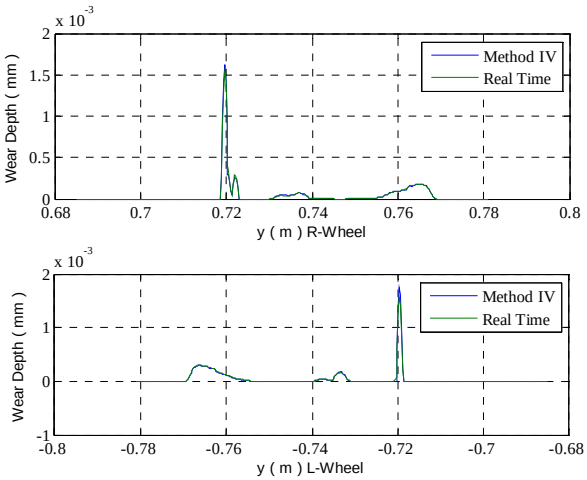

Figure 22: Comparison between Method IV & Real Time of wear depth evolution after 13 km on both wheel profiles.

2.10 Effect of vehicle velocity:

The same simulation has been performed using different velocities 10 m/s and 25 m/s with a 13000 km distance, a 200 multiplier and using rail inclination angle of 1:40 , and the results were plotted in Fig. 23.

The effect of velocity is reasonable, in fact at higher velocity creepages and normal loads are higher and subsequently the wear rate increase. Furthermore at higher velocity, the centrifugal forces push the wheelset in lateral direction and wear occurs towards the flange. At low speed wear is located mainly n the tread (at 10 m/s) for the left wheel flange wear disappear.

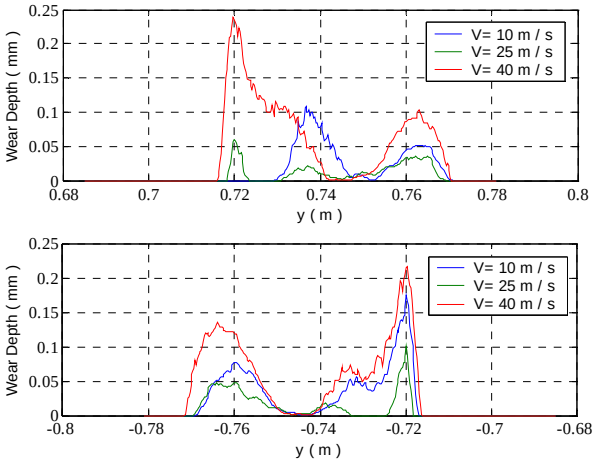

Figure 23: The effect of the running velocity on the wear rate and wear behavior using 1:40 rail inclination angle (up left, down right wheel).

2.11 Effect of track irregularities:

On figure 24, the worn depths are compared for the vehicle running at 40 m/s with 1:40 rail inclination with and without track irregularities. Track irregularities have been measured on a real track with the same topology of the one described in this work. The irregularities, measured every 0.1 m, consist in track alignment errors (lateral, vertical and roll) and gauge irregularities, while theoretical rail profiles have been used.

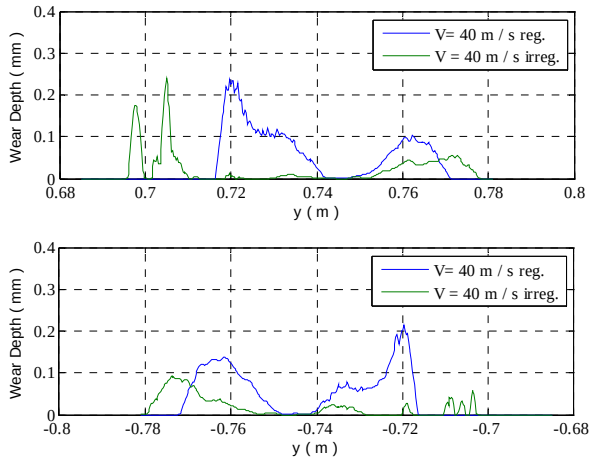

Figure 24: The effect of track irregularity on the wear depth with 1:40 inclination angle.

The effect of track irregularities is important: it heavily change both wear depth and its location on the profile. In particular it is evident that flange contact occurs more frequently, since track irregularities increases the lateral motion of the wheelset

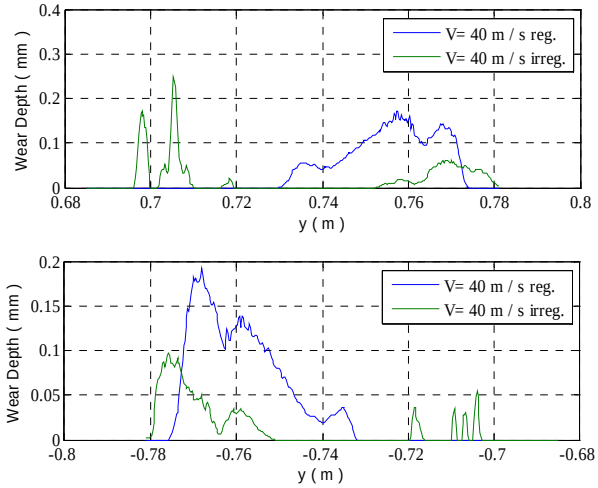

Figure 25: The effect of track irregularity on the wear depth with 1:20 inclination angle.

3. CONSIDERATIONS

3.1 Simulation Statistics :

Table 2 shows the time required for a full simulation using method IV with different multipliers, 13000 km and 1:20 and 1:40 inclination angles. Simulations are performed using an Intel Pentium 4 2.4 MHz processor with the Windows XP OS.

It is clear that is convenient to use a multiplier as high as possible. In the following we will analyze how this multiplier can affect the results.

Incl. Angle	Multiplier	Hour	Minute	Second
1:40	10	43	29	1
	100	2	43	48
	200	1	23	54
	500	0	34	8
	1000	0	21	1
1:20	10	30	17	23
	100	3	11	25
	200	1	17	33
	500	0	16	49
	1000	0	23	29

Table 2: Time calculations for Method IV using different multipliers.

3.2 Error estimation:

a- comparison of various methods with 13000 km, 1:40 & 1:20 rail inclination angle

A comparison between the various methods is made on a length of 13000 km with the 10 multiplier. Results are shown in Figure 26; we could conclude that the III and IV method give the same results, which are reasonably correct based on the previous comparison made between real time simulation and method IV. While method II had given good results of wear depth only on the tread. The reason is that using constant displacement classes, the statistical significance is lost because some classes are ill populated and other overpopulated. On the other hand, Method I, is typically constant wear case, which is far from the reality and can not be considered for the calculation of wear distribution.

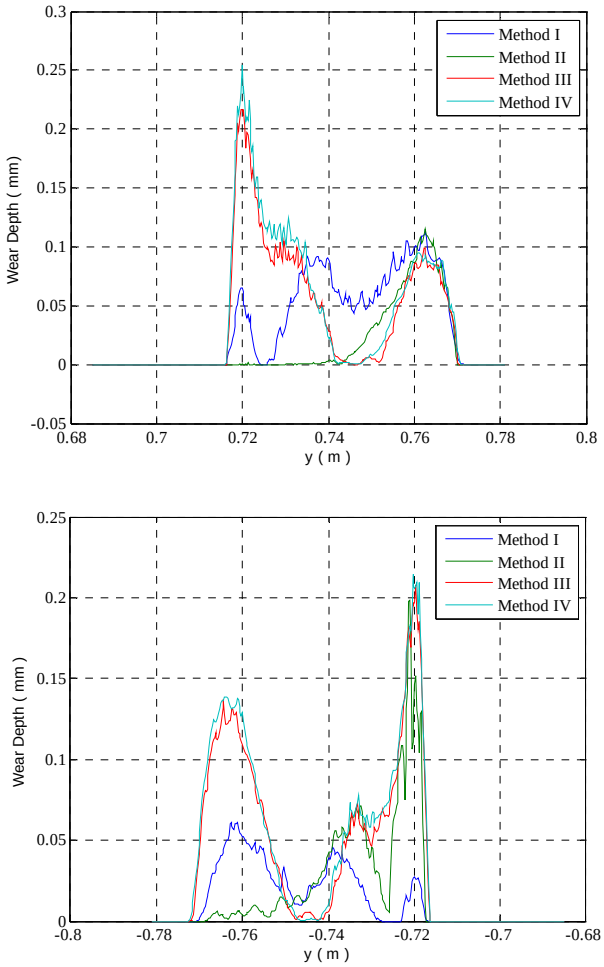

Figure 26 Comparison of the various methods with multiplier=10 with 1:40 inclination angle.

Now, a comparison between the various multipliers has been done for the method IV, in order to roughly estimate which are the multipliers that could give better results, for both inclination angles, as shown in Fig.27.

Actually, it is very marked that the 500 and 1000 multipliers diverge the results very rapidly. Therefore, They can be excluded from being used in further simulations.

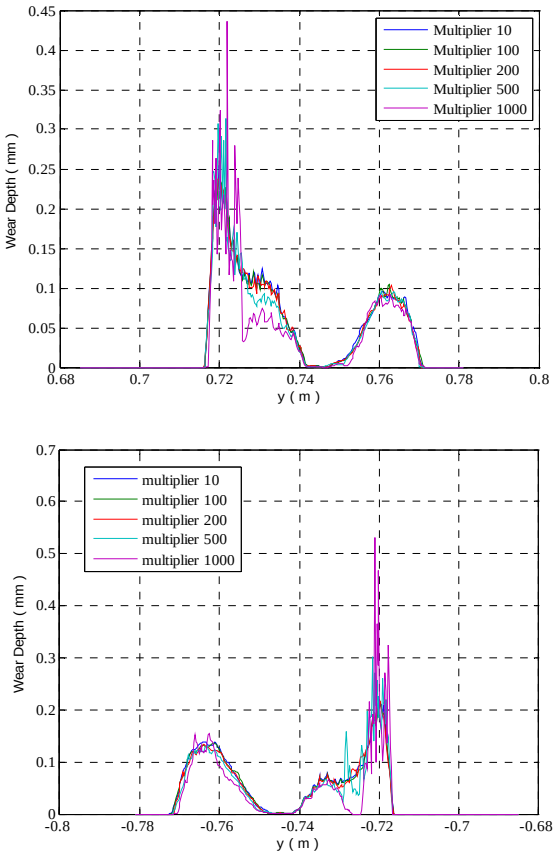

Figure 27 Comparison of various multipliers with 1:40 inclination angle using Method IV.

b- Optimal multiplier determination

In order to select the optimum multiplier, the error has been calculated by determining the area under the curve in Fig. 27, 28, and then all the areas are compared to the area of the curve with multiplier 10, which would give the best results as described before. Therefore, the multiplier 10 was put as a zero percent error, and the errors of all the other multipliers were calculated with respect to it. As the intervals in the y-direction are constants, the area under the curve can be calculated from the sum of the wear depths. In this way, the error calculated will is based on the amount of material lost. The error equation used is:

$$Error\% = \left(\sum_j \Gamma_m - \sum_j \Gamma_{10} \right) \Big/ \sum_j \Gamma_{10} \times 100 \qquad (22).$$

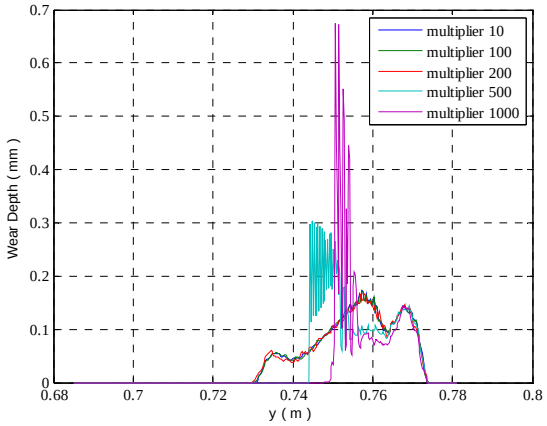

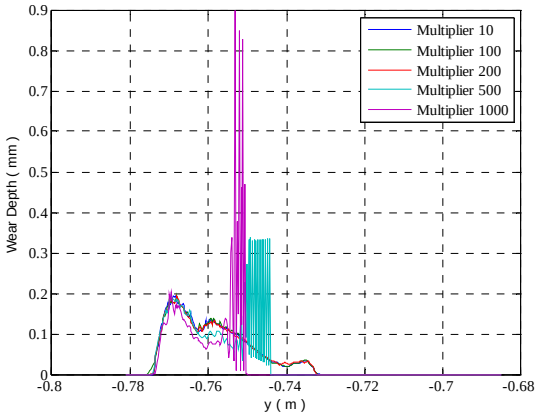

Figure 28 Comparison of various multipliers with 1:20 inclination angle using Method IV.

The results obtained are shown in table 3, in which we could conclude that the maximum error in the calculation of the wear depth is (-18.7%).

As it was already clear from the diagrams of fig. 27 and 28, the multiplier shod be chosen lower than 500. This consideration cannot be derived from the material loss, but from the wear distribution along the profile, that for values higher than 200 shows a sharp increment in flange depth of wear.

W-side	pos	Multiplier					
		10	100	200	400	500	1000
R	1:20	0	-18,7%	-1,0%	-2,8%	-1,8%	-18,7%
L		0	-9,6%	-0,6%	5,5%	-9,6%	-0,6%
R	1:40	0	-1,3%	-2,8%	-1,8%	-5,5%	-14,5%
L		0	-1,8%	-4,1%	-1,9%	-1,8%	-4,1%

Table 3: Error in Percentage for Method IV Using Different Multipliers and Different Rail Inclination.

In terms of wear depth, table 4 shows a comparison across the different methods. Methods I appear clearly inadequate, while III and IV are substantially equivalent.

Method II gives better results than method I but against an higher computational time (more classes) is not efficient as methods VI and III.

Wheel side	Incl. angle	Method I	Method II	Method III	Method IV
Right	1:40	0,061	0,198	0,208	0,214
Left		0,11	0,115	0,217	0,254
Right	1:20	0,011	-	-	0,194
Left		0,027	-	-	0,173

Table 4: Maximum Wear Depth. Comparison between different methods with a 13000 km simulation and different rail inclination.

3.3 Effect of rail inclination over wear shape:

As shown in Fig. 29, the effect of the rail inclination angle is visible. These results are obtained from a simulation of 130000 km with both angles by method IV. It is evident that with 1:40 inclination the wear rate is higher at the face and lower at the flange border than that of 1:20 inclination.

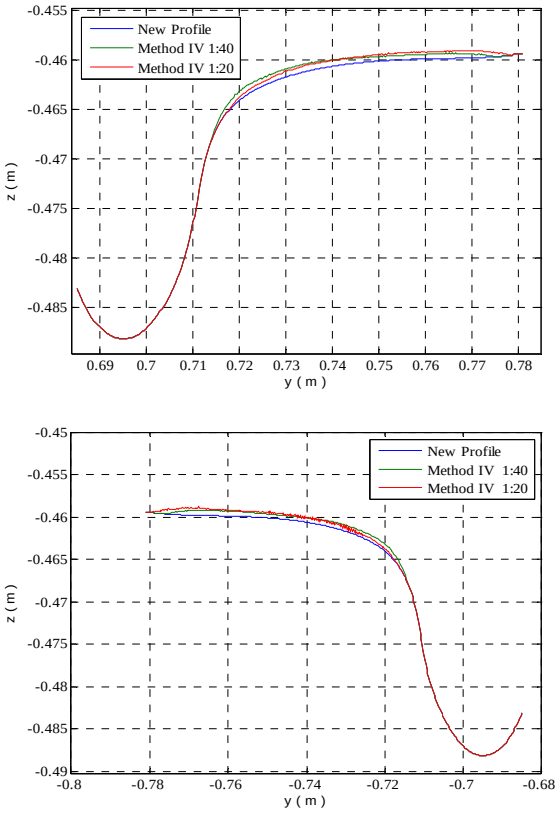

Fig. 29 Comparison of worn profiles simulation results of Method IV with different inclination angles, 1:40 & 1:20.

3.4 Conclusions

In this work, a method to determine wear depth and distribution over a railway wheel profile has been shown.

The method has been developed in order to achieve a reasonable efficiency, in order to be able to simulate the effect of long mileage realistic tracks on a wheelset.

The problem was approached developing simple statistical methods, to group the dynamic data in order to be representative of the entire track at a desired level of accuracy.

Different methods are compared starting from numerical data obtained on a reference track. Error and efficiency has been quantified for each method. The simulations show that is possible to determine a "multiplier" of the wear rate, which is a good compromise between accuracy and time consumption.

"Quality" of the method is also very important, since even if all methods give reasonable results in terms of total worn material (max error 20% in the worst case), the wear distribution vary in an important manner.

Main limitation of a "statistical" approach is that the wear of the profile cannot affect dynamic of the wheelset. In fact dynamic simulation are performed separately respect the wear analysis (Contact point and stresses are re-calculated but obviously the dynamic data are not changed because the wear process is evaluated on the "class" domain and not on the time domain). The effect of the worn profiles on the dynamic of the vehicle has not been considered in this work.

REFERENCES

[1] Bolton, P. J., and Clayton, P., 1994, "Rolling-Sliding Wear Damage in Rail and Tyre Steels," J. Wear, 93, pp. 145-165.

[2] Kimura, Y., Sekizawa, M., and Nitanai, A., 2002, "Wear and Fatigue in rolling contact," J. Wear, 253, pp. 9–16.

[3] Krause, H., and Poll, G., 1986, "Wear and Fatigue in rolling contact," J. Wear, 113, pp. 103-122.

[4] Lewis, R., Cavalletti, M., Dwyer-Joyce, R.S., Ward, A., Bruni, S., Bel Knani, K., and Bologna, P., 2002, "Railway Wheel Wear Predictions with Adams/Rail," 1st MSC.ADAMS European User Conference, London, 13-14 November.

[5] Steel, R. K., and Reif, R., 1982, "Rail: Its Behavior and Relationship to Total System Wear," J. Colorado Springs, pp. 227–276.

[6] Kalker, J. J., 1990, "Simulation of the Development of a Railway Wheel Profile Through Wear," J. Wear, 150, pp. 335–365.

[7] Danks, D., and Clayton, P., 1987, "Comparison of the Wear Processes for Eutectoid Rail Steels: Field and Laboratory Tests," J. Wear, 120, pp. 233-255.

[8] Kalker, J. J., 1982, "A Fast Algorithm for the Simplified Theory of Rolling Contact," J. Vehicle System Dynamics, 11, pp. 1–13.

[9] Sarkar, A. D., 1976, Wear of Metals, First edition.

[10] Rabinowicz, E., 1995, Friction and Wear, second edition, John Whiley & Sons Inc.

[11] Garg, V. K., and Dukkipati, R. V., 1984, Dynamics of Railway Vehicle Systems, Academic Press, Ontario, Canada, Chap. 4 & 5.

[12] N. Bosso, A. Gugliotta, A. Somà, "Introduction of a wheel-rail and wheel-roller contact model for independent wheels in a Multibody code." Proceedings of the IEEE/ASME Joint Railroad Conference 2002 , pp. 151-159.

[13] N. Bosso, A. Gugliotta, L. Gusman, A. Somà. "Simulazione del comportamento dinamico di una sala ferroviaria per Roller-Rig" - XXIX AIAS - Lucca 6-9 Settembre 2000.

[14] J.J. Kalker; "Three-dimensional elastic bodies in rolling contact", Dordrecht, Kluwer Academic Publishers, 1990.

[15] K.L. Johnson; "Contact Mechanics", Cambridge University Press, 1985.

[16] A.D. de Pater; "The geometrical contact between track and wheelset." Vehicle System Dynamics, Vol. 17 (1988), pp. 127-140.

[17] Question ORE C116- Rp6; "Geometry of the contact between wheelset and track." Office for Research and Experiments. Utrecht, 1976-04-01.